Imaging Hot Paper

Deutsche Ausgabe: DOI: 10.1002/ange.201603945
Internationale Ausgabe: DOI: 10.1002/anie.201603945

Cross-Platform DNA Encoding for Single-Cell Imaging of Gene Expression

*Pavel Zrazhevskiy, Shreeram Akilesh, Wanyi Tai, Konstantin Queitsch, Lawrence D. True, Jonathan Fromm, David Wu, Peter Nelson, John A. Stamatoyannopoulos, and Xiaohu Gao**

Abstract: *Integration of imaging data across different molecular target types can provide in-depth insight into cell physiology and pathology, but remains challenging owing to poor compatibility between target-type-specific labeling methods. We show that cross-platform imaging analysis can be readily achieved through DNA encoding of molecular targets, which translates the molecular identity of various target types into a uniform in situ array of ssDNA tags for subsequent labeling with complementary imaging probes. The concept was demonstrated through multiplexed imaging of mRNAs and their corresponding proteins with multicolor quantum dots. The results reveal heterogeneity of cell transfection with siRNA and outline disparity in RNA interference (RNAi) kinetics at the level of both the mRNA and the encoded protein.*

Gaining access to detailed "molecular portraits" of individual cells within the context of their natural cell culture or tissue microenvironment promises to revolutionize biomedical research and dramatically advance clinical diagnostics and drug discovery.[1–3] A number of imaging platforms have been developed for the comprehensive analysis of individual types of molecular targets, particularly proteins, mRNA, and DNA.[4–12] However, simultaneous analysis across different target types remains challenging owing to poor compatibility between target-type-specific labeling methods, and is further restricted by additional requirements imposed by the imaging probe properties.

[*] Dr. P. Zrazhevskiy, Dr. W. Tai, Prof. X. Gao
Department of Bioengineering, University of Washington
Seattle, WA 98195 (USA)
E-mail: xgao@uw.edu
Dr. S. Akilesh, Prof. L. D. True
Department of Pathology, University of Washington
Seattle, WA 98195 (USA)
K. Queitsch, Prof. J. A. Stamatoyannopoulos
Department of Genome Sciences, University of Washington
Seattle, WA 98195 (USA)
Prof. J. Fromm, Prof. D. Wu
Department of Laboratory Medicine, University of Washington
Seattle, WA 98195 (USA)
Prof. P. Nelson, Prof. J. A. Stamatoyannopoulos
Department of Medicine, University of Washington
Seattle, WA 98195 (USA)
Prof. P. Nelson
Fred Hutchinson Cancer Research Center
Seattle, WA 98109 (USA)

Supporting information for this article can be found under: http://dx.doi.org/10.1002/anie.201603945.

Herein, we describe a versatile cross-platform single-cell imaging technology that enables simultaneous visualization of multiple molecular targets irrespective of the target type and imaging probe used. An essential step to achieving cross-platform compatibility is the implementation of an indirect labeling method built on the concepts of 1) decoupling of the target binding and labeling steps, 2) translation of heterogeneous molecular information into an intermediate standardized molecular code that can be read through the use of imaging probes, and 3) utilization of the enormous encoding capacity and self-assembly capabilities of DNA that result from complementary base pairing.[13,14] Specifically, molecular targets of interest are first encoded with unique ssDNA tags through binding by ssDNA-conjugated target-recognition moieties under optimized conditions that favor strong and specific target binding. Individual ssDNA tags are then converted into detectable signals through sequence-specific hybridization with complementary ssDNA′-conjugated imaging probes under probe-optimized conditions. Molecular target uniqueness, localization, and abundance, and information on specimen morphology are thus preserved through all steps of the labeling procedure, thereby producing comprehensive molecular signatures of a physiological or pathological process. It should be emphasized that this method is not meant to be applied to the study of DNAs, RNAs, or proteins in a massive parallel fashion. Instead, it aims to enable the interrogation of a panel of selected genomic, transcriptomic, and/or proteomic markers in single cells by bringing them onto the same imaging platform.

To demonstrate the DNA encoding concept for imaging molecular targets across different types, we performed a concurrent assessment of molecular expression at both the mRNA and protein levels (Figure 1), which is one of the most actively explored approaches for the evaluation of gene regulation, cell signaling, RNA–protein interactions, and many other applications.[15–19] Fluorescent quantum dot probes (QDots)[20–22] in combination with fluorescence microscopy and hyperspectral imaging (HSI)[23,24] were employed for simultaneous visualization of all of the ssDNA tags following separate encoding of mRNA and protein targets (Figure 1 a). Unlike direct labeling procedures performed under a single set of incubation conditions that are fixed for all targets and probes,[25–27] DNA encoding enables tuning of the conditions to favor the recognition of individual target types and hybridization with detection probes in separate steps, which offers great flexibility in the choice of specimens, targets, and imaging systems. Conceptually, any combination of target-specific affinity moieties and imaging probes should be amenable to coupling via intermediate

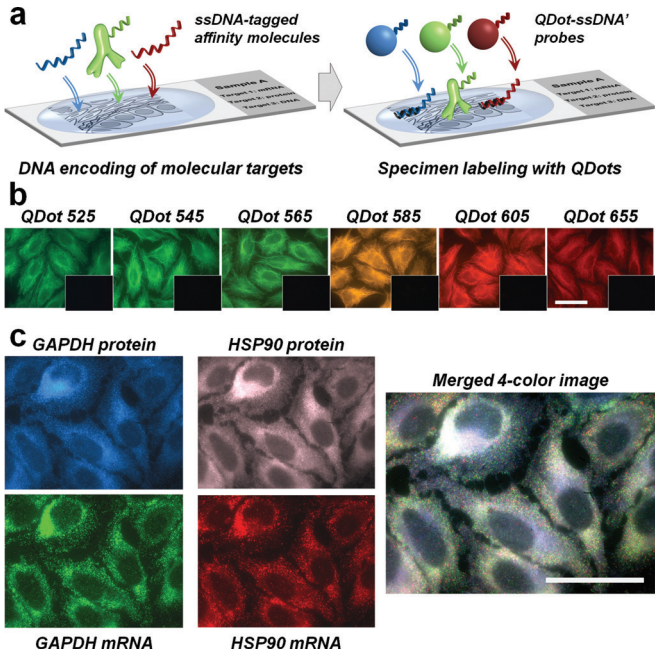

Figure 1. a) Schematic of simultaneous labeling and multiplexed imaging of different molecular targets with multicolor QDots through DNA encoding. Each molecular target is encoded by a target-specific ssDNA-tagged affinity molecule, and the resulting array of target-bound ssDNA tags is sequentially or simultaneously labeled with complementary imaging probes. b) Staining of β-tubulin with a panel of 6-color QDot–ssDNA′ probes. The target was first encoded through anti-β-tubulin primary antibody and ssDNA-conjugated rabbit anti-mouse secondary antibody, followed by hybridization with complementary QDot–ssDNA′ probes. Insets: control experiments skipping incubation with primary and secondary antibodies rule out non-specific QDot binding. True-color images for target staining vs. control were obtained at consistent exposure time for each QDot color. c) Multiplexed labeling of GAPDH and HSP90-alpha mRNA and corresponding proteins (with QDots 605, 655, 585, and 545). The ssDNA tags were simultaneously converted into distinctive optical signals through hybridization with complementary QDot–ssDNA′ probes. Fluorescence microscopy with HSI was employed for cell imaging and unmixing of 4 individual QDot channels. Individual grayscale channels were false-colored and merged into a composite 4-color image. Scale bar: 50 μm.

DNA tags, thus rendering this technology useful for broader multi-omics imaging studies.

To implement and systematically characterize the model QDot-based cross-platform imaging technology, a set of 6 unique 16 bp ssDNA/ssDNA′ linkers was designed for encoding up to 6 different molecular targets (Table S1 in the Supporting Information), along with a library of complementary 6-color QDot–ssDNA′ probes (Figure S1 in the Supporting Information) and a control set of 6 secondary antibody (2′Ab)–ssDNA bioconjugates (Figure S2). Indirect labeling of β-tubulin in HeLa cells through a 3-step procedure involving incubation with unmodified primary antibodies, 2′Ab–ssDNA bioconjugates, and complementary QDot–ssDNA′ probes demonstrated preserved antigen-recognition functionality of the ssDNA–modified antibodies and high specificity of QDot staining through DNA hybridization (Figure 1b).

Multiplexed protein immunolabeling was realized through the preparation of a library of primary antibody (1′Ab)–ssDNA bioconjugates (Figures S3, S4). Characterization of such bioconjugates through PAGE and cell staining confirmed preserved stability and antigen-binding functionality of antibodies, specificity of target staining with QDots in a 2-step procedure, and consistent target identification with different QDot colors in a multiplexed imaging format (Figure S4b–e). The nuclear envelope protein Lamin A, the microtubule protein β-tubulin, and the cytoplasmic proteins HSP90-alpha and GAPDH were labeled as model target molecules with distinct and characteristic intracellular localization patterns.

Labeling of the GAPDH and HSP90-alpha mRNAs through indirect in situ hybridization (ISH) was done with modified mRNA ISH oligonucleotide probes featuring a 5′ 20 nt mRNA-recognition portion and a 3′ 16 nt QDot-binding tag, separated by a single-stranded AAAAA spacer (Tables S2, S3). Hybridization of oligonucleotide probes under optimized ISH conditions yielded labeling of each mRNA molecule with multiple ssDNA tags (up to 36 for GAPDH and 48 for HSP90-alpha), which produce distinct "spots" upon staining with complementary QDot–ssDNA′ probes (Figure S5).

The separation of target-recognition and QDot-labeling events through DNA encoding enabled straightforward implementation of a model cross-platform imaging method, with both mRNA and protein targets being robustly labeled by their respective QDot probes and accurately identified through hyperspectral imaging and analysis. For example, GAPDH and HSP90-alpha mRNA molecules and their respective product proteins could be readily labeled with 4-color QDots to highlight the relative intracellular distribution and abundance of the two target types at the single-cell level (Figure 1c), thus corroborating the broad applicability of the DNA encoding strategy for the simultaneous detection and imaging of various types of targets within the same specimen.

The cross-platform imaging approach was then applied to study RNA interference (RNAi)-mediated gene knockdown at the single-cell level. HeLa cells were transfected with GAPDH-targeting small interfering RNA (siRNA), as well as non-targeting siRNA as a control, for 24 h, and the abundance of GAPDH mRNA was assessed by reverse transcription polymerase chain reaction (RT-PCR) and QDot-based imaging. Interestingly, single-cell imaging revealed complete degradation of GAPDH mRNA (Figure 2a), whereas bulk GAPDH mRNA measurement by RT-PCR indicated a silencing efficiency of only 78% with forward (on surface) transfection and 95% with reverse (in suspension) transfection. Imaging at the cell population level revealed the basis for this discrepancy: heterogeneous knockdown of the target mRNA in a subset of cells, which likely results from heterogeneous cell transfection with the siRNA in different regions of cell culture (Figure 2b,c). For example, forward transfection failed to achieve efficient GAPDH mRNA degradation in dense cell populations (at the well edges), yielding areas of completely silenced cells along with patches of cells with normal GAPDH mRNA expression levels (Figure 2b). In contrast, reverse transfection achieved a more uniform cell

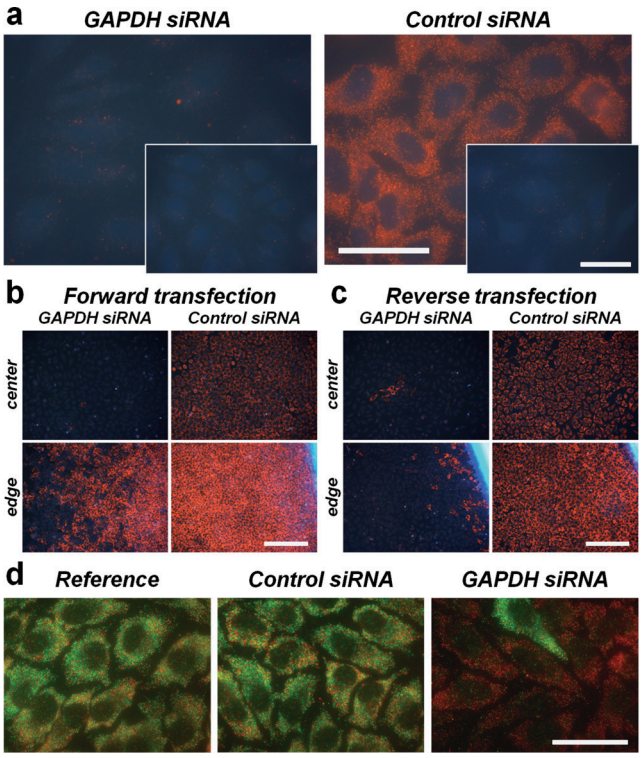

Figure 2. Assessment of heterogeneity in cell transfection with siRNA. a) Complete degradation of GAPDH mRNA was observed at the single-cell level after a 24 h treatment with GAPDH-targeting siRNA (left panel), whereas non-targeting control siRNA had no effect on GAPDH mRNA abundance (right panel). Insets: control experiments with mismatched QDot605-ssDNA′ probes establish the level of non-specific background labeling. Scale bar: 50 μm. b,c) Heterogeneity of GAPDH silencing is observed in different areas of the culture well (center vs. edge) with forward transfection but not with reverse transfection (labeling with QDot605 probes). Occasional colonies with full GAPDH expression can be observed with both transfection methods. Scale bar: 250 μm. d) Dual-labeling of GAPDH and HSP90-alpha mRNA with QDot565 and QDot585, respectively, enables direct visualization of RNAi on different targets. After a 24 h treatment with GAPDH siRNA, the majority of the cells show complete degradation of the GAPDH mRNA (right panel, green), but retain unperturbed HSP90-alpha mRNA (right panel, red). A single cell in the field of view (green) has apparently failed to be transfected with GAPDH siRNA and features normal mRNA expression. Dual-color images were obtained with HSI, unmixed into QDot channels, and false-colored. Scale bar, 50 μm.

transfection in suspension, producing a greater proportion of silenced cells with only a few wild-type clones (Figure 2c).

The selectivity of the GAPDH RNAi was confirmed by performing dual-target imaging of GAPDH mRNA and HSP90-alpha mRNA. Target-selective siRNA should trigger degradation of only its complementary target mRNA, with no immediate effect on non-targeted mRNA molecules. This was indeed observed with GAPDH RNAi studies (Figure 2d and Figure S6). Indirect dual-target ISH produced robust staining of both mRNA species in reference HeLa cells grown in culture medium. Similarly, cell transfection with non-targeting control siRNA failed to produce any effect on mRNA expression. Transfection with GAPDH-targeting siRNA, however, triggered rapid degradation of GAPDH mRNA within 24 h post-transfection, while leaving non-targeted HSP90-alpha mRNA intact. Notably, a single non-transfected cell within the field of view featured intact expression of both GAPDH and HSP90 mRNA, thus suggesting an all-on/all-off mode for GAPDH RNAi.

Imaging of mRNA unambiguously demonstrated heterogeneity in RNAi knockdown, which likely stems from incomplete cell transfection with the siRNA. However, such heterogeneity could not be detected at the protein level, since levels of GAPDH protein remained unperturbed 24 h post-transfection in both transfected and non-transfected cells, as was evident from dual labeling of GAPDH mRNA and protein (Figure S7). To further investigate the disparity between the RNAi effect at the mRNA and protein levels, HeLa cells were reverse transfected with GAPDH-targeting siRNA for 24 and 48 h and processed for multiplexed imaging of GAPDH and HSP90-alpha mRNA and their respective protein products. Consistent with studies discussed earlier, 24 h post-transfection, complete degradation of GAPDH mRNA was observed, whereas GAPDH protein level remained nearly unperturbed (Figure 3a). By contrast, 48 h post-transfection, a substantial reduction of GAPDH protein levels was observed, with GAPDH mRNA remaining below the detection limit (Figure 3b). HSP90 mRNA and protein levels remained unperturbed over 48 h, thus confirming the selectivity of GAPDH silencing. Furthermore, all of molecular targets exhibited consistent unperturbed levels in cells

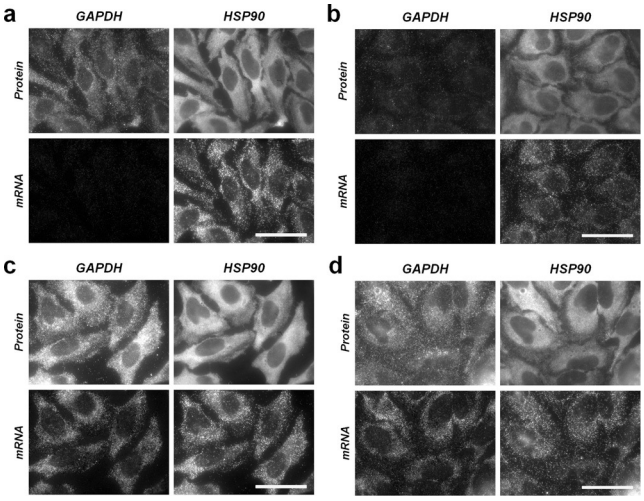

Figure 3. Assessment of the disparity in RNAi knockdown kinetics at the mRNA and protein levels. HeLa cells were transfected with GAPDH siRNA (a, b) or control siRNA (c, d) for 24 h (a, c) or 48 h (b, d). GAPDH and HSP90-alpha mRNA along with corresponding proteins were simultaneously assessed (labeling with QDots 605, 655, 585, and 545). a) There is complete and selective degradation of GAPDH mRNA 24 h post-transfection, whereas the GAPDH protein levels remain nearly unperturbed. b) 48 h post-transfection, selective degradation of GAPDH protein can be observed. c, d) With control (non-targeting) siRNA, GAPDH and HSP90 expression at the mRNA and protein levels remain constant through 48 h of incubation. Multiplexed images were obtained through HSI, and individual channels are normalized to the HSP90 protein channel for direct comparison of signal intensity. Scale bar: 50 μm.

transfected with non-targeting control siRNA (Figure 3c,d), thus confirming that the observed GAPDH knockdown indeed resulted from RNAi mechanism.

A delay in the RNAi effect at the protein level is not surprising, since proteins are typically degraded and cleared more slowly in comparison to siRNA-mediated mRNA degradation. However, in light of the imaging results presented here, heterogeneity in cell transfection needs to be taken into consideration when assessing RNAi efficiency with bulk RT-PCR measurements and especially downstream phenotypic and molecular signaling analysis. Non-transfected cells might gain a growth advantage and achieve substantial clonal expansion during the time it takes for higher-level manifestations of RNAi to occur, thus distorting observed RNAi effect at the population level. Imaging-based analysis at the single-cell level should, therefore, offer more accurate insight into cellular response to perturbation.

In conclusion, the cross-platform imaging technology presented herein enables simultaneous in situ detection and visualization of multiple types of molecular targets at the single-cell level. Decoupling of target recognition and labeling events and conversion of heterogeneous molecular information into a uniform intermediate ssDNA array amenable to read-out with variety of imaging probes represents a key technological advance towards gaining access to single-cell molecular profiles through multi-omics imaging, which might be challenging, if not impossible, to achieve through the simple combination of conventional labeling methods (e.g., immunofluorescence and in situ hybridization). Importantly, the DNA code can be readily converted into a digital read-out through simple hybridization to multiplexed imaging probes, thereby offering a universal link between multitudes of available selective target-recognition moieties and emerging powerful multiplexed imaging platforms. This cross-platform DNA encoding technology is thus expected to facilitate the development of novel single-cell imaging methods and the implementation of molecular profiling studies across different target types in biomedical research, drug development, and clinical diagnostics.

Acknowledgements

This work was supported in part by NIH (R01CA131797, R21CA192985) and the Department of Bioengineering at the University of Washington. S.A. is a Damon Runyon Fellow supported by the Damon Runyon Cancer Research Foundation (DRG-114-13). P.Z. thanks the National Cancer Institute for a T32 fellowship (T32CA138312).

Keywords: DNA encoding · gene expression · imaging · quantum dots · single-cell measurements

How to cite: *Angew. Chem. Int. Ed.* **2016**, *55*, 8975–8978
Angew. Chem. **2016**, *128*, 9121–9124

[1] R. A. Burrell, N. McGranahan, J. Bartek, C. Swanton, *Nature* **2013**, *501*, 338.
[2] P. L. Bedard, A. R. Hansen, M. J. Ratain, L. L. Siu, *Nature* **2013**, *501*, 355.
[3] M. G. Krebs, R. L. Metcalf, L. Carter, G. Brady, F. H. Blackhall, C. Dive, *Nat. Rev. Clin. Oncol.* **2014**, *11*, 129.
[4] M. Angelo, S. C. Bendall, R. Finck, M. B. Hale, C. Hitzman, A. D. Borowsky, R. M. Levenson, J. B. Lowe, S. D. Liu, S. Zhao, Y. Natkunam, G. P. Nolan, *Nat. Med.* **2014**, *20*, 436.
[5] K. H. Chen, A. N. Boettiger, J. R. Moffitt, S. Wang, X. Zhuang, *Science* **2015**, *348*, aaa6090.
[6] R. Jungmann, M. S. Avendano, J. B. Woehrstein, M. Dai, W. M. Shih, P. Yin, *Nat. Methods* **2014**, *11*, 313.
[7] F. Porichis, M. G. Hart, M. Griesbeck, H. L. Everett, M. Hassan, A. E. Baxter, M. Lindqvist, S. M. Miller, D. Z. Soghoian, D. G. Kavanagh, S. Reynolds, B. Norris, S. K. Mordecai, Q. Nguyen, C. Lai, D. E. Kaufmann, *Nat. Commun.* **2014**, *5*, 5641.
[8] E. C. Stack, C. Wang, K. A. Roman, C. C. Hoyt, *Methods* **2014**, *70*, 46–58.
[9] P. Zrazhevskiy, X. Gao, *Nat. Commun.* **2013**, *4*, 1619.
[10] C. Giesen, H. A. Wang, D. Schapiro, N. Zivanovic, A. Jacobs, B. Hattendorf, P. J. Schuffler, D. Grolimund, J. M. Buhmann, S. Brandt, Z. Varga, P. J. Wild, D. Gunther, B. Bodenmiller, *Nat. Methods* **2014**, *11*, 417.
[11] H. M. Choi, J. Y. Chang, A. Trinh le, J. E. Padilla, S. E. Fraser, N. A. Pierce, *Nat. Biotechnol.* **2010**, *28*, 1208.
[12] M. J. Gerdes, C. J. Sevinsky, A. Sood, S. Adak, M. O. Bello, A. Bordwell, A. Can, A. Corwin, S. Dinn, R. J. Filkins, D. Hollman, V. Kamath, S. Kaanumalle, K. Kenny, M. Larsen, M. Lazare, Q. Li, C. Lowes, C. C. McCulloch, E. McDonough, M. C. Montalto, Z. Pang, J. Rittscher, A. Santamaria-Pang, B. D. Sarachan, M. L. Seel, A. Seppo, K. Shaikh, Y. Sui, J. Zhang, F. Ginty, *Proc. Natl. Acad. Sci. USA* **2013**, *110*, 11982.
[13] M. R. Jones, N. C. Seeman, C. A. Mirkin, *Science* **2015**, *347*, 1260901.
[14] V. Tjong, L. Tang, S. Zauscher, A. Chilkoti, *Chem. Soc. Rev.* **2014**, *43*, 1612.
[15] A. P. Frei, F. A. Bava, E. R. Zunder, E. W. Hsieh, S. Y. Chen, G. P. Nolan, P. F. Gherardini, *Nat. Methods* **2016**.
[16] I. Weibrecht, E. Lundin, S. Kiflemariam, M. Mignardi, I. Grundberg, C. Larsson, B. Koos, M. Nilsson, O. Soderberg, *Nat. Protoc.* **2013**, *8*, 355.
[17] J. Xiu, Q. Zhang, T. Zhou, T. T. Zhou, Y. Chen, H. Hu, *Nat. Neurosci.* **2014**, *17*, 1552.
[18] H. Xu, L. A. Sepulveda, L. Figard, A. M. Sokac, I. Golding, *Nat. Methods* **2015**, *12*, 739.
[19] S. Darmanis, C. J. Gallant, V. D. Marinescu, M. Niklasson, A. Segerman, G. Flamourakis, S. Fredriksson, E. Assarsson, M. Lundberg, S. Nelander, B. Westermark, U. Landegren, *Cell. Rep.* **2016**, *14*, 380.
[20] E. Petryayeva, W. R. Algar, I. L. Medintz, *Appl. Spectrosc.* **2013**, *67*, 215.
[21] K. D. Wegner, N. Hildebrandt, *Chem. Soc. Rev.* **2015**, *44*, 4792.
[22] P. Zrazhevskiy, M. Sena, X. Gao, *Chem. Soc. Rev.* **2010**, *39*, 4326.
[23] R. M. Levenson, A. Fornari, M. Loda, *Expert Opin. Med. Diagn.* **2008**, *2*, 1067.
[24] L. D. True, X. Gao, *J. Mol. Diagn.* **2007**, *9*, 7.
[25] M. de Planell-Saguer, M. C. Rodicio, Z. Mourelatos, *Nat. Protoc.* **2010**, *5*, 1061.
[26] M. Gasnier, C. Dennis, C. Vaurs-Barriere, C. Chazaud, *Nat. Protoc.* **2013**, *8*, 2538.
[27] S. G. Zimmerman, N. C. Peters, A. E. Altaras, C. A. Berg, *Nat. Protoc.* **2013**, *8*, 2158.

Received: April 23, 2016
Published online: June 7, 2016

